Dalton Transactions

Luminescent Properties of a 3,5-diphenylpyrazole Bridged Pt(II) Dimer

Journal:	*Dalton Transactions*
Manuscript ID	DT-ART-02-2019-000795.R1
Article Type:	Paper
Date Submitted by the Author:	22-Mar-2019
Complete List of Authors:	Cinninger, Leander; Univ Texas Austin, Chemistry; Intel Corporation Bastatas, Lyndon; The University of Texas at Dallas, Physics; Oklahoma State University, Physics Shen, Yulong; The University of Texas at Dallas, Physics; Qorvo, Inc. Holliday, Bradley; BJH Consulting Slinker, Jason; The University of Texas at Dallas, Physics

Journal Name

RSCPublishing

ARTICLE

Luminescent Properties of a 3,5-diphenylpyrazole Bridged Pt(II) Dimer†

Cite this: DOI: 10.1039/x0xx00000x

Leander M. Cinninger,[a,b] Lyndon D. Bastatas[c,d] Yulong Shen,[c,e] Bradley J. Holliday[f] and Jason D. Slinker*[c]

Received 00th January 2012,
Accepted 00th January 2012

DOI: 10.1039/x0xx00000x

www.rsc.org/

We report the synthesis, electrochemistry, photophysical properties and incorporation of a highly luminescent pyrazolate-bridged platinum (II) complex into light-emitting electrochemical devices. The complex has the general formula of $[((N\hat{}C\hat{}N)Pt)_2(\mu\text{-pz})][PF_6]$ where N^C^N = 1,3-di(2-pyridyl)benzene and μ-pz = 3,5-diphenylpyrazolate. The X-ray structure shows that the bridging pyrazolate ligand causes a close Pt-Pt interaction of 3.057 Å. The emission profile of the complex was determined in solution, glassy 2-methyltetrahydrofurane at 77 K, and the solid state at both room temperature and 77 K. Each emission profile displayed a strong red metal-metal-to-ligand charge transfer while the solution and glassy 2-methyltetrahydrofurane emission profiles also displayed a ligand-centred transition. The absolute quantum yields of the complex in solution and the solid state at room temperate are 86% and 39%, respectively. Light-emitting electrochemical cells (LEECs) of $[((N\hat{}C\hat{}N)Pt)_2(\mu\text{-pz})][PF_6]$ were fabricated which displayed appreciable electroluminescence, among the brightest and most efficient LEECs from dinuclear compounds to date.

Introduction

Square-planar platinum (Pt) complexes have been extensively researched due to their numerous potential applications as chemosensors[1,2], photocatalysts[3–8] and as materials in optoelectronic[9–11] and photovoltaic[12–14] devices. Pt complexes that use a cyclometalating ligand are often luminescent in solution at room temperature and can display a wide range of optical properties. The strong σ-donating ability of the cyclometalating ligand forces the metal-centered d-d excited states higher in energy, removing this efficient, radiationless decay pathway and allowing for highly luminescent molecules. Due to the unsaturated dz^2 orbital on square-planar Pt complexes, many show excimer or aggregate formation, leading to a red shifting in emission when compared to the mononuclear species. This type of red shifted emission is typically denoted as a metal-metal-to-ligand charge transfer (MMLCT) or excimer ligand-to-ligand charge transfer. A MMLCT transition is a charge transfer between a filled Pt-Pt antibonding orbital and an empty, ligand-based π* orbital. Pt complexes can be designed to possess a bridging ligand, which forces these mononuclear species into permanent close contact with each other, creating permanent emission from MMLCT transitions and highly luminescent materials. The use of bis-phosphino[15] and pyrazolate[15–19] ligands as bridging groups has been studied by several groups.

In this study, we report the synthesis (Scheme 1) and characterization of the novel, highly luminescent pyrazolate-bridged cyclometalated platinum(II) complex **3** which has the formula $[((N\hat{}C\hat{}N)Pt)_2(\mu\text{-pz})][PF_6]$ (where N^C^N = 1,3-di(2-pyridyl)benzene and μ-pz = 3,5-diphenylpyrazolate). We incorporated this device into light emitting electrochemical cells (LEECs) and discuss their feasibility for optoelectronic applications.

Results and discussion

Synthesis

The cyclometalating ligand **1** was synthesized using a Negishi coupling of 2-bromopyridine to 1,3-dibromobenzene.[20] Metalation using potassium tetrachloroplatinate and acetic acid afforded the intermediate complex **2**.[21] The chloride ligand on **2** was replaced with the bridging 3,5-diphenylpyrazole ligand by first deprotonating the pyrazole followed by the addition of complex **2** to generate the resulting pyrazolate bridged platinum(II) dimer **3**. Anion exchange was performed using KPF_6 to replace the chlorine counter ion with a PF_6. Anion exchange was performed in order to prevent the chlorine counter ion from degrading the product by displacement of the pyrazolate ligand.

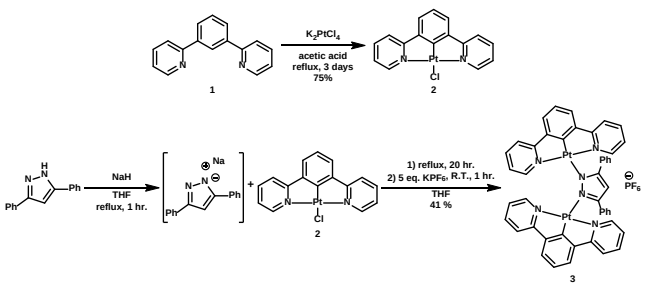

Scheme 1. Synthesis of complex **2** and complex **3**.

X-ray crystal structures

The single-crystal X-ray structure of **3** has been determined and is shown in Figure 1. Two square-planar Pt moieties are bridged by the μ-3,5-diphenylpyrazolate ligand. The steric bulk on the 3 and 5 postitions of the μ-pyrazolate ligand forces the two N^C^N ligands closer together, creating favorable interactions of the dz^2 orbitals of the two Pt centers. The Pt-Pt distance in **3** is 3.057 Å, which is well within the 2.8-3.6 Å range for Pt-Pt interactions. The phenyl groups on the μ-pyrazolate ligand show a slight twist away from the plane of the pyrazolate backbone, which is in conjunction with the slight staggering of the square-planar Pt moieties. The separation of the N^C^N ligands ranges from 3.2 Å near the Pt centers to 3.9 Å at the outer edge of the N^C^N ligands. These distances are within the typical range for π-π interactions, which can be seen with the stacking of the N^C^N ligands. The use of bridging pyrazolate ligands with bulky R-groups at the 3 and 5 positions to create close Pt-Pt interactions has been previously reported.[16]

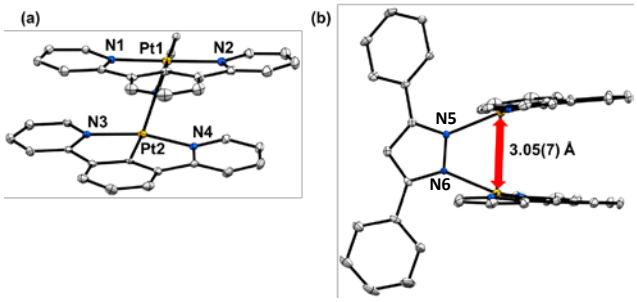

Figure 1. Oak Ridge Thermal Ellipsoid Plot **(**ORTEP) views of **3** with 50% ellipsoid probability: (a) Phenyl rings on the 3 and 5 positions of the μ-pyrazolate have been removed for clarity. (b) Side view of **3** to show Pt-Pt interaction and stacking of the N^C^N ligands.

Electrochemical properties

Cyclic voltammetry was used to evaluate the redox potentials of **3**; the graph of which is provided in the supporting information (figure S2-S3). The values reported are relative to a ferrocenium/ferrocene reference. Complex **3** showed an irreversible oxidization at $E_{p,a}$ = 0.74 V which was coupled to a reduction at $E_{p,c}$ = -0.26 V. There were also two other reversible reductions at more negative potentials ($E_{p,c}$ = -2.03 V, $E_{p,c}$ = -2.27 V). It is believed that oxidation is localized on the metal center, while reduction occurs mainly on the N^C^N ligands, which is consistent with reports on related Pt(II) complexes.[22] Overall, **3** has an experimentally measured HOMO/LUMO band gap of 2.46 eV.

Photophysical properties

The UV-Visible absorption spectrum of **3** in DCM (Figure 2a) shows two bands below 300 nm ($\varepsilon > 70 \times 10^3$ M^{-1} cm^{-1}), two bands between 350 nm and 425 nm ($\varepsilon > 10 \times 10^3$ M^{-1} cm^{-1}), and two bands between 440 nm and 540 nm ($\varepsilon > 2 \times 10^3$ M^{-1} cm^{-1}). The broad, featureless bands below 300 nm are due to π-π* transitions localized on the N^C^N ligands, while the intense bands between 350 nm and 425 nm are attributed to ^{1}MMLCT transitions. The two peaks between 440 nm and 540 nm are due to the ^{3}MMLCT transitions. These results are consistent with similar systems reported by Che *et al.*,[15] and Catellano *et al.*[18] The experimentally measured band gap from the UV-Visible spectrum of **3** is 2.38 eV, which is comparable to the electrochemically determined band gap.

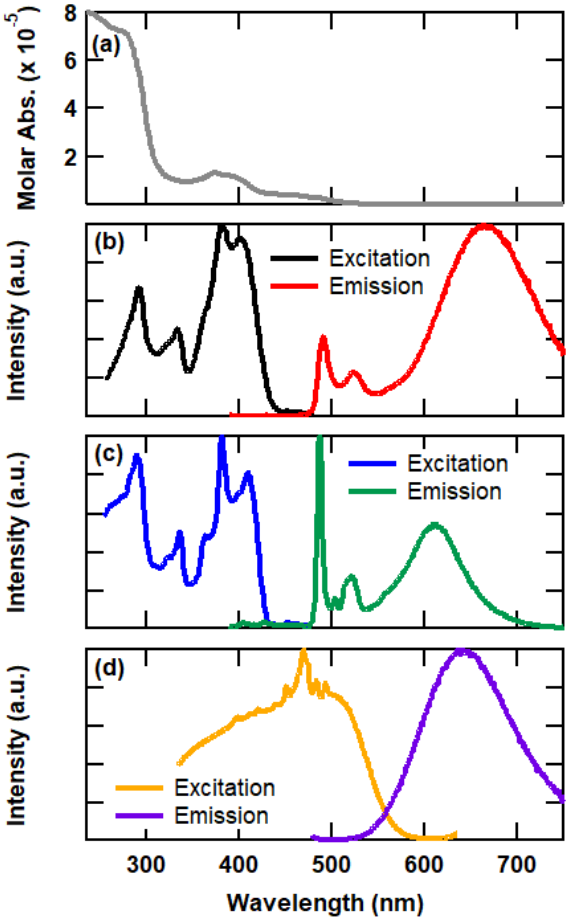

Figure 2. Molar absorptivity, absorption, and emission profiles of **3**. (a) Molar absorptivity of **3** in DCM (RT). Emission and excitation profiles of **3**: (b) DCM (RT), (c) 2-MeTHF (77 K), and (d) solid state (powder, RT).

Complex **3** emits in solution and solid state at both room temperature and 77 K. The excitation and emission profile **3** in solution at 77 K and room temperature along with the solid-state excitation and emission profile at room temperature are displayed in Figure 2. The emission spectrum of **3** in DCM at room temperature shows two different transitions upon excitation at 380 nm. The first of which is at 490 nm and has a luminescent lifetime (τ) in the microsecond regime ($\tau = 6.9 \pm 0.5$ μs). Due to the microsecond τ and the clear vibronic progression of this peak, it was assigned as the triplet ligand-centered (^{3}LC) transition from the N^C^N ligand, which matches previously reported data on the chloride contained precursor **2**.[22] The second transition is a broad, structureless peak centered at 664 nm and has a $\tau = 4.6 \pm 0.8$ μs. This transition has been assigned as the

triplet metal-metal-to-ligand charge transfer (^{3}MMLCT) transition. This type of transition is common in other reports of dinuclear Pt(II) complexes with close Pt-Pt interactions.[15,18,19] Overall, **3** is highly emissive in solution with an absolute quantum yield of 86 %.

The emission profile of **3** in 2-MeTHF glass at 77 K when excited at 380 nm is similar to that displayed in DCM at room temperature. There is a ^{3}LC transition at 487 nm (τ = 7.0 ± 0.5 μs) and a ^{3}MMLCT transition at 612 nm (τ = 4.7 ± 0.8 μs), which is blue shifted by 53 nm in comparison to the ^{3}MMLCT transition at room temperature in DCM. Other reported dinuclear Pt(II) complexes also show blue shifting of the ^{3}MMLCT transition when lowered to 77 K.[15] Complex **3** emits green in color when dissolved in 2-MeTHF at 77 K, but rapidly turns to orange upon warming. This physical observation is supported by the emission spectrum of **3** in 2-MeTHF glass, where the ^{3}MMLCT transition is less dominant in intensity in comparison to the ^{3}LC transition. As the solution begins to warm to room temperature, the ^{3}MMLCT transition begins to become more and more dominant, causing the color shift from green emission to orange emission.

The emission profile of **3** when excited at 470 nm in the solid state (powder) at room temperature and 77 K was also studied. Both solid state emission spectra showed that the ^{3}LC transition had been completely quenched, showing only a broad ^{3}MMLCT transition. This transition was centered at 643 nm (τ = 3.3 ± 0.9 μs) at room temperature and 639 nm (τ = 2.8 ± 1.4 μs) at 77 K (figure S5). The room temperature ^{3}MMLCT is blue shifted by 29 nm in comparison to that in solution due to a destabilization of the excited state while in the solid state. However, based on previous work reported by Che *et al.*, where the 77 K solid state ^{3}MMLCT in their dinuclear Pt(II) systems are red shifted in contrast to the room temperature emission,[15] the 77 K ^{3}MMLCT transition of **3** is slightly blue shifted in comparison to the room temperature ^{3}MMLCT. To further understand why this might be the case, variable temperature single-crystal X-ray diffraction was used to study the Pt-Pt distances in **3**. The single-crystal structure of **3** was collected at 100 K, 150 K, 200 K, and 250 K. The Pt-Pt distances of **3** between these four temperatures only showed a slight variation of 0.01 Å, as evident from the Figure 3 overlap of the structures at 100 K and 250 K. This observation may be due to complex **3** having a more rigid structure, causing there to be very little contraction of the Pt-Pt distances in the crystal lattice at 77 K. The room temperature absolute quantum yield of **3** in the solid state (Φ_{solid} = 39 %) is significantly lower than in solution, presumably due to quenching caused by the close packing of the solid in comparison to in solution.

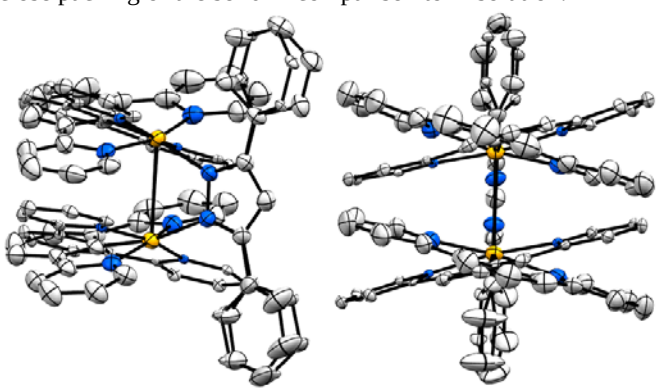

Figure 3. Overlay of the Pt centers of the single crystal structures of **3** at 100 K and 250 K with 50% ellipsoid probability.

Electroluminescent properties

Electroluminescence (EL) spectra were recorded for LEEC devices from pristine films and films augmented with 0.3%/wt $LiPF_6$ (Figure 4). The $LiPF_6$ ionic additive has been shown to improve response time, luminance, and efficiency metrics through improved ion mobility and enhancing double layer formation at the cathode.[23-26] (Due to these effects, arising from the small Li^+ cation, we chose $LiPF_6$ over $BMIMPF_6$,[27-28] an additive commonly used to improve response times. Ionic liquids of smaller cations can have similar effects to $LiPF_6$.[28]) The pristine device shows a broad peak consistent with a ^{3}MMLCT transition with a maximum at 695 nm. This is redshifted by 50 nm with respect to the solid-state film. Alternatively, the ionic additive device also exhibits a broad-spectrum indicative of a ^{3}MMLCT transition, but with a peak at 665 nm, considerably closer to the PL max.

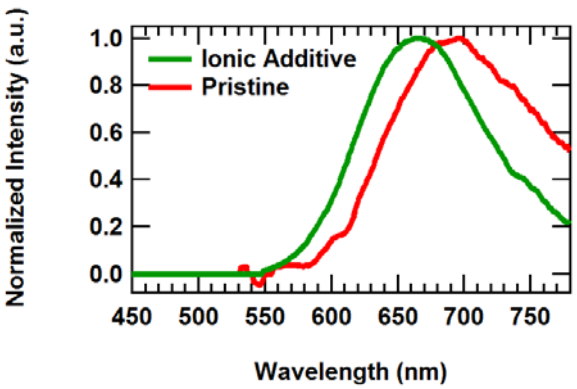

Figure 4. Electroluminescence spectra of [**3**][PF6] LEEC devices with (Ionic Additive) and without (Pristine) 0.3% $LiPF_6$.

Electroluminescence in LEECs occurs within a thin region of the film between the electrodes as dictated by the relative injection efficiencies and mobilities of electrons and holes.[29-33] The large spectral shift of the pristine device likely indicates that the EL emission zone is offset from the center and occurring in regions of high ionic space charge content where the electric field is high, such that the spectral shift is a Stark shift. Adding the ionic additive likely moves the location of the emission zone closer to the center of the device by balancing carrier injection to bring about emission more closely matching the thin film photoluminescence. This postulate can be further explored through study of the relative luminance and efficiency of the devices.

The luminance versus time graph of LEECs from **3** running at constant current is shown in Figure 5. The pristine device shows a slow onset of emission that maximizes after ~2 hr near 10 cd/m^2, then slowly decays with a half-life of approximately 13 hr. The maximum external quantum efficiency is less than 0.05% photons/electron for this device, a low value anticipated from the irreversibility of oxidation. Nonetheless, lithium salt addition improves the performance. The maximum luminescence of the ionic additive device is enhanced twofold relative to the pristine device to 20 cd/m^2. The $LiPF_6$ ioinc additive raises the maximum quantum efficiency to 0.22%. The onset of emission is seen almost immediately, and the luminance maximum is achieved in 30 s. This suggests that the ionic additive helps to balance carrier concentrations. This observation

could also reconcile the EL spectra of Figure 4, as postulated above. The higher maximum efficiency and luminance of the ionic additive device is consistent with more balanced carrier injection. This ionic additive device, in turn, is more likely to produce an emission zone in the bulk and an emission spectrum more in line with that predicted from photoluminescence, as observed in Figure 4. Overall, this demonstrates that Pt dimers such as **3** can produce appreciable electroluminescence as LEEC devices.

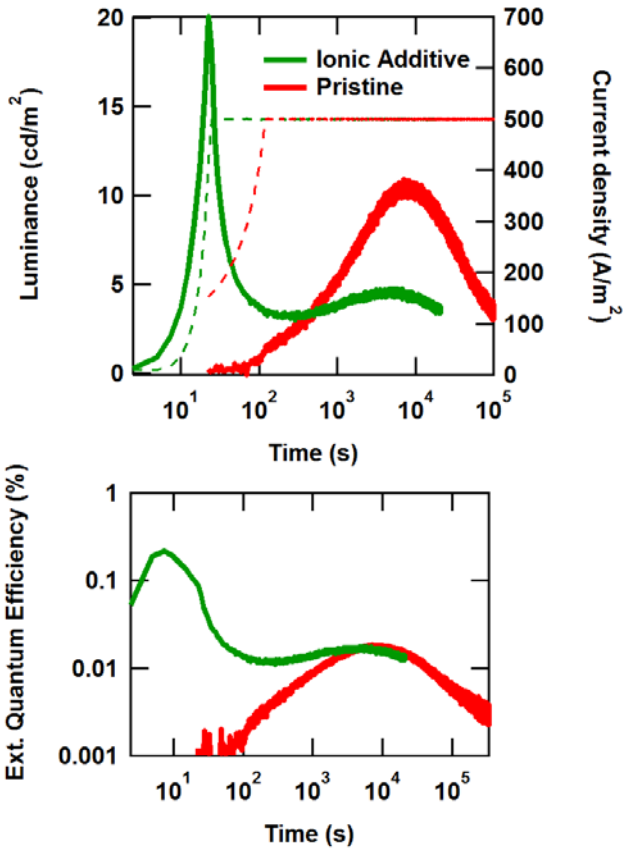

Figure 5. Luminance (upper, solid lines), current density (upper, dashed lines) and external quantum efficiency (lower) vs. time plot of LEEC devices from **3** with (Ionic Additive) and without (Pristine) 0.3% $LiPF_6$ at 1.5 mA constant current (500 A/m^2 current density).

Interestingly, this ionic additive device exhibits a transient maximum that is followed by a second, more gradual increase to a maximum of 5 cd/m^2. The transient 20 cd/m^2 maximum occurs precisely at the transition from bias-limited to current-limited driving (Fig. 5). That is, in the early stages of operation, the 10V bias compliance is reached as the devices are highly resistive. As ionic redistribution occurs, the device resistance is lowered as efficient charge injection is established. The rapid rise of the luminance is aided by the high potential across the device. When the current limit is reached, the bias must be lowered to maintain constant current. For an injection limited contact, decreasing the bias can exponentially lower the injected current, and so this lowered bias can decrease current balance, lowering luminance and efficiency until a new steady state is established. Interestingly, a second luminance peak emerges and decays on the same timescale of the pristine device (half-life of 14 h), which likewise occurs under steady state conditions. This effect is not unique to these materials, as we have observed similar dynamics with some LEECs from mononuclear iridium complexes, particularly when large voltages are invoked for extended times. Dynamics are also likely impacted by the susceptibility of these materials to oxidative damage, as suggested by electrochemistry, a feature that could be somewhat alleviated with a bilayer approach.[34-36] Nonetheless, electroluminescence emerges, suggesting further improvements in stability could yield practical electroluminescent materials. Indeed, previous study of mononuclear Pt complexes in LEECs among a series of metal centers (Pt, Zn, Sn) showed them to exhibit promising external quantum efficiency among the sequence, but lower stability.[37] Thus, early work of Pt emitters in light emitting electrochemical cells suggests that understanding of stability is the key to advancing their use.

Among LEECs from ionic transition metal complexes (iTMCs),[38-44] other groups have followed the effects of binuclear complexes in LEECs. Leprêtre *et al.* investigated a binuclear ruthenium complex with the addition of lithium salts and crown ether solid electrolytes.[45] In this system, no luminance was observed with the pristine device, nor with lower amounts of the ether/salt mixture. Above a threshold of electrolyte/salt addition, the device operated at 0.02% external quantum efficiency. Wang *et al.* used a binuclear ruthenium complex to achieve near IR emission at 790 nm, but with efficiency estimated at 0.0005%.[46] Likewise, Wang *et al.* demonstrated bias-dependent emission from a copper complex, emitting 590 nm centered emission under forward bias and 618 nm emission under reverse bias.[47] Absolute luminance and efficiency values were not reported. Costa *et al.* reported LEEC performance from a series of dumbbell-shaped dinuclear iridium complexes. Luminance was low (<10 cd/m^2), and a maximum quantum efficiency of 0.16% was observed from the series.[48] Thus, the performance of this dinuclear LEEC based on **3** (maximum 20 cd/m^2, 0.22% external quantum efficiency) is noteworthy among this series.

Conclusions

In summary, the 3,5-diphenylpyrazolate bridged Pt(II) dimer **3** was synthesized and fully characterized. The X-ray diffraction determined molecular structure of **3** shows a close Pt-Pt interaction of 3.057 Å. Cyclic voltammetry shows an oxidation which is associated with the Pt centers and a reduction which is associated with the pyridine rings of the cyclometallating ligands. The photophysical properties of **3** show the presence of a ^{3}LC and a ^{3}MMLCT transition in both the room temperature solution state and in 77 K 2-MeTHF glass while the emission profile of **3** in the solid state at both room temperature and 77 K shows only a ^{3}MMLCT band which is blue-shifted from the ^{3}MMLCT present in the solution. Complex **3** was used as the luminescent material in an LEEC device, showing electroluminescence of 20 cd/m^2 in the presence of $LiPF_6$. To the best of our knowledge, this is the first reported example of using a Pt dimer as the luminescent material in an LEEC. Further improvements in complex stability against oxidative damage could potentially increase the electroluminescence of the Pt dimer LEEC devices.

Experimental procedures

Materials and methods

All air and moisture-sensitive reactions were performed using standard Schlenk and high vacuum techniques. All dry solvents were dried using an Innovative Technology, Pure Solv solvent purifier with a double purifying column and setting over 3 Å molecular sieves for 48 hours. All chemicals were used as received without further purification. The ^{1}H NMR was recorded on a Varian Unity 300 spectrometer (300 MHz) and the ^{13}C NMR was recorded on Varian DirectDrive 400 spectrometer (400 MHz). All NMR peaks are reported in ppm and all coupling constants are reported in Hz. Infrared spectra were recorded on a Nicolet iS50 FT-IR spectrophotometer. Low-resolution and high-resolution mass spectrometry was performed on an Agilent Technologies 6530 Accurate Mass QTofLC/MS spectrometer. Melting points were recorded on an OptiMelt Automated Melting Point System made by Stanford Research Systems. Elemental analysis was performed by Midwest MicroLab Inc. (Indianapolis, IN).

N^C^NPt(μ-pz)PtN^C^N (3)

In dry Schlenk flask, 3,5-diphenylpyrazole (48 mg, 0.22 mmol) and of NaH (12 mg of 60% NaH suspended in paraffin oil, 0.30 mmol) were dissolved in dry THF (20 mL). The solution was stirred for one hour at room temperature then **2** (200 mg, 0.43 mmol) was added to the flask. The reaction was heated to 76 °C and stirred for 20 hours. The reaction was cooled to room temperature then potassium hexafluorophosphate (400 mg, 1.73 mmol) was added to the flask. The reaction was stirred for an additional hour. The THF was removed under reduced pressures, then the resulting solid was washed with cold DI water (2 x 10 mL). The resulting brown solid was collected by filtration then washed with diethylether (2 x 10 mL). The solid was dissolved in CH_2Cl_2 (20 mL), then filtered through a pad of celite to remove any insoluble impurities. The product was purified via recrystallization from CH_2Cl_2 using hexanes, resulting in a bright orange solid (215 mg, 0.18 mmol, 41%). The solid glows orange upon excitation with a long-wave UV lamp (λ_{max} = 365 nm). m.p. 250-302 °C (slow decomp.), FTIR (solid): 1608 cm^{-1} (m, aromatic stretch). ^{1}H NMR (300.14 MHz, CD_2Cl_2): δ 8.57 (d (unresolved additional splitting), *J*=7.5 Hz, 4H), 7.85 (d (unresolved additional splitting), *J*=7.5 Hz, 4H), 7.71 (t (unresolved additional splitting), *J*=7.5 Hz, 4H), 7.63 (s, 1H), 7.44-7.22 (m, 10H), 7.20-7.06 (m, 6H), 6.68 (t (unresolved additional splitting), *J*=7.75 Hz, 4H). ^{13}C NMR (100.53 mHz, CD_2Cl_2) δ 167.40, 162.23, 153.21, 151.41, 141.42, 139.90, 132.92, 129.23, 128.34, 126.54, 124.48, 124.23, 123.49, 120.26, 103.79. HRMS (ESI) m/z calculated for $C_{47}H_{33}N_6Pt_2$ 1071.9978 $[M]^+$, found 1071.2159. Elemental analysis calculated for $C_{47}H_{33}F_6N_6PPt_2$ (1216.96): C, 46.39; H, 2.73; N, 6.91. Found: C, 46.41; H, 2.64; N, 6.86.

Electrochemistry

All electrochemical experiments were completed under nitrogen in a glovebox using a GPES system from Eco. Chemie B. V. and an Autolab Potentiostat. The electrolyte used was 0.1 M tetrabutylammonium hexafluorophosphate, $[(n\text{-Bu})_4N][PF_6]$ ($TBAPF_6$) in either dry ACN or dry DCM. The electrolyte was purified through three recrystallizations from hot ethanol before drying under active vacuum for three days at 100 °C. Electrochemical experiments of **3** were carried out in a 20 mL electrochemical using a platinum button working electrode (1.6 mm diameter), a $Ag/AgNO_3$ (0.01 M $AgNO_3$ and 0.1 M $TBAPF_6$ in dry ACN) non-aqueous reference electrode, and a Pt wire coil counter electrode. All potentials were reported relative to ferrocene, which was used as an external standard to calibrate the reference electrode. The ferrocene was purified by sublimation at 95 °C. A step potential of 10 mV and a scan rate of 100 mV s^{-1} were used unless otherwise noted. The band gap was determined from the difference between the onset of oxidation (HOMO) and the onset of reduction (LUMO).

Photophysical measurements

Solvents used for emission, excitation, and lifetime studies were degassed using the conventional freeze-pump-thaw method under N_2 atmosphere. Absorption spectra were recorded on a Varian Cary 6000i UV-VIS-NIR spectrophotometer and did not require degassed solvents. Luminescent measurements were recorded using FeliX32 software with a BryteBox interface on a Photon Technology International (PTI) QuantaMaster 4 spectrophotometer equipped with a 6-inch diameter K Sphere-B integrating sphere. Steady-state luminescence spectra were measured by exciting the sample with a xenon short arc lamp (USHIO, UXL-75XE) connected to a PTI lamp power supply (LPS-250B) and recording the emission with a PTI detection system (model 814) using a photomultiplier tube (Hamamatsu, R928P). Time-resolved luminescence spectroscopy was used to measure the excited-state lifetimes by exciting the sample with a xenon flash lamp (Hamamatsu, L4633), connected to a PTI XenoFlash power supply, and recording the decay using a photomultiplier tube (Hamamatsu, R562).

All solution measurements were recorded with the samples in Starna quartz fluorimeter cells with a path length of 1 cm. For solution spectra, **3** was dissolved in the desired solvent and diluted until the UV-Vis absorbance was below 0.1. For solid spectra, the solid was ground into a powder and loaded into either the main box (PTI, K-149) or the sphere powder holder (PTI, K-205). Frozen spectra were taken using a fluorimeter dewar (Wilmad Glass Co., Inc.) with a Suprasil quartz sample tube, which fits into the cuvette dewar holder (PTI, K-158) in the spectrophotometer. Samples were made by slowly freezing a solution of **3** dissolved in 2-methyltetrahydrofuran (2-MeTHF) in an EPR tube with liquid nitrogen in the fluorimeter dewar. Optical filters from Edmund Industrial Optics were used where specified.

All quantum yield measurements were recorded using the integrating sphere. For solution quantum yields, the concentration of the solution was maximized to the point before concentration quenching of the emission occurred. Quantum yields were calculated by dividing the area under the emission peak of the complex by the difference between the area under the excitation peak of the sample from that of a blank solution ($A_{em\ sample}$ /($A_{ex\ blank} - A_{ex\ sample}$), where A = area under peak).[49] The reported quantum yields are an average of three trials.

Crystal structure determination

The crystallographic data for complex **3** is given in Table S1-S4. Single crystals of **3** were grown via slow vapor diffusion of diethyl ether into a solution of **3** in dichloromethane. The single crystal covered in a Paratone/chloroform mixture and mounted on a nylon thread loop. The single crystal X-ray diffraction data was collected at 100K, 150 K, 200 K, and 250 K. All single crystal XRD data was collected with an Agilent Technologies SuperNova Dual Source diffractometer using a μ-focus Cu Kα radiation source (λ = 1.5418 Å) equipped with collimating mirror monochromators. Data collection, unit cell refinement, and data

reduction were performed using the Agilent Technologies CrysAlisPro.[50] The structure of **3** was solved by direct methods using the SIR2014[51] program and refined by full-matrix least-squares on F^2 with anisotropic displacement parameters for all non-H atoms using SHELXL-2013.[52] The structural analyses were performed using the PLATON98[53] and WinGX[54] programs. The hydrogen atoms were placed in fixed, calculated positions with isotropic displacement parameters set to 1.2 x U_{eq} with respect to the attached atom. Crystallographic images were created using the Mercury[55] and rendered using POV-ray.[56]

Device preparation and characterization

The overall LEEC device composition is as follows: ITO/PEDOT:PSS/Active Layer/LiF/Al. Active layers of **3** were tested with and without the 0.3% $LiPF_6$ salt additive. $LiPF_6$ was purchased from Sigma Aldrich in the highest available purity and used as received. Prepatterned ITO-coated glass substrates were purchased from Thin Film Devices, Anaheim, CA. These substrates were cleaned in a non-ionic detergent and water bath, followed by UV ozone treatment. Aqueous PEDOT:PSS solutions (1.3 – 1.7%, Clevios AI 4083) were filtered through a 0.45 μm GHP filter and then spin coated (~20 nm thick) onto the ITO-coated glass substrates. The substrates were subsequently transferred into a dry nitrogen glovebox for further processing and characterization. Separate solutions of **3** and $LiPF_6$ were each prepared at a concentration of 24 mg/mL in degassed acetonitrile inside the glovebox. For the devices with the 0.3% $LiPF_6$ additives, these $LiPF_6$ salt and iTMC solutions were subsequently mixed at a volume ratio of 3 to 997, respectively. The final solutions were then heated on a hotplate at 85 °C while stirring for 10 minutes and allowed to cool down to room temperature before being passed through a 0.1 μm nylon filter. The iTMC films, with and without $LiPF_6$, were spin cast at 900 rpm and thermally annealed at 120 °C for 1 hour. The active layers were generally ~100 nm thick. Then the samples were transferred to a vacuum chamber, where 10 Å of LiF and 800 Å of Al were deposited through a shadow mask that defined 12 devices per substrate, each with a 3 mm^2 active area.

The electrical and radiant flux characteristics were obtained with a custom LEEC multiplexer testing station capable of measuring 16 device slides simultaneously. In brief, this instrument served as a current or voltage source and measuring unit and captured radiant flux with a calibrated Hamamatsu photodiode (S2387-1010R) for each device. The device slides were driven at a constant current of 1.5 mA (10 V compliance). These results were verified against measurements obtained with a 760D electrochemical analyzer from CH Instruments (Austin, TX) and a calibrated Labsphere integrating sphere, equipped with a thermoelectric cooled silicon photodetector and Keithley 6485 Picoammeter. Electroluminescence spectra were measured from thin film single layer devices with an Ocean Optics Jazz fiber spectrometer.

Conflicts of Interest

There are no conflicts of interest to declare.

Acknowledgements

JDS acknowledges support from a gift from Qorvo, Inc. BJH gratefully acknowledges the Welch Foundation (F-1631) and the National Science Foundation (CHE-0847763) for financial support of this research.

Notes and references

[a] *Department of Chemistry, The University of Texas at Austin, Austin, TX 78712, USA.*
[b] *Intel Corporation, Portland, OR 97124, USA.*
[c] *Department of Physics, The University of Texas at Dallas, 800 W. Campbell Rd, Richardson, TX 75080, USA.* *E-mail: slinker@utdallas.edu*
[d] *Department of Physics, Oklahoma State University, Stillwater, Oklahoma, USA, 74078*
[e] *Qorvo, Inc., 500 W. Renner Rd., Richardson, TX 75080, USA.*
[f] *BJH Chemical Consulting, Austin, TX 78735.*

† Electronic Supplementary Information (ESI) available: X-ray crystal data and structure refinement of **3**, UV-Vis absorption spectra, and electrochemical CVs.

1 C. S Peyratout, T. K. Aldridge, D. K.Crites and D. R. McMillin, *Inorg. Chem.* 1995, **34**, 4484.
2 S. W. Thomas III, K. Venkatesan, P.Müller and T. M. Swager, *J. Am. Chem. Soc.* 2006, **128**, 16641.
3 D. Zhang, L.-Z. Wu, L.Zhou, X. Han, Q.-Z. Yang, L.-P. Zhang and C.-H. Tung, *J. Am. Chem. Soc.* 2004, **126**, 3440.
4 H. Ozawa, M.-A. Haga and K. Sakai *J. Am. Chem. Soc.* 2006, **128**, 4926.
5 K. Sakai, H. Ozawa, *Coord. Chem. Rev.* 2007, **251**, 2753.
6 H. Ozawa and K. Sakai *Chem. Commun. (Camb).* 2011, **47**, 2227.
7 X. Wang, S. Goeb, Z. Ji, N. A. Pogulaichenko and F. N. Castellano *Inorg. Chem.* 2011, **50**, 705.
8 M. Kobayashi, S. Masaoka and K. Sakai, *Angew. Chemie - Int. Ed.* 2012, **51**, 7431.
9 B. W. D'Andrade, J. Brooks, V. Adamovich, M. E. Thompson and S. R. Forrest, *Adv. Mater.* 2002, **14**, 1032.
10 W. Lu, B.-X. Mi, M. C. W. Chan, Z. Hui, C.-M. Che, N. Zhu and S.-T. Lee, *J. Am. Chem. Soc.* 2004, **126**, 4958.
11 W.-Y. Wong, Z. He, S.-K. So, K.-L. Tong and Z. Lin, *Organometallics* 2005, **24**, 4079.
12 J. E. McGarrah and R. Eisenberg, *Inorg. Chem.* 2003, **42**, 4355.
13 Y. Shao and Y. Yang, *Adv. Mater.* 2005, **17**, 2841.
14 W.-Y. Wong, X.-Z. Wang, Z. He, A. B. Djurisić, C.-T. Yip, K.-Y. Cheung, H. Wang, C. S. K. Mak and W. K. Chan, *Nat. Mater.* 2007, **6**, 521.
15 S.-W. Lai, M. C.-W. Chan, T. C. Cheung, S.-M. Peng and C.-M. Che, *Inorg. Chem.* 1999, **38**, 4046.
16 B. Ma, J. Li, P. I. Djurovich, M. Yousufuddin, R. Bau and M. E. Thompson, *J. Am. Chem. Soc.* 2005, **127**, 28.
17 S. Cho, M. W. Mara, X. Wang, J. V. Lockard, A. A. Rachford, F. N. Castellano and L. X. Chen, *J. Phys. Chem. A* 2011, **115**, 3990.
18 A. Chakraborty, J. C. Deaton, A. Haefele and F. N. Castellano, *Organometallics* 2013, **32**, 3819.
19 M. Han, Y. Tian, Z. Yuan, L. Zhu and B. Ma, *Angew. Chemie Int. Ed.* 2014, **53**, 10908.
20 Katagiri, S.; Sakamoto, R.; Maeda, H.; Nishimori, Y.; Kurita, T.; Nishihara, H. *Chemistry* **2013**, *19*, 5088–5096.
21 D. J. Cárdenas and A. M. Echavarren, *Organometallics* 1999, **18**, 3337.

22 Z. Wang, E. Turner, V. Mahoney, S. Madakuni, T. Groy and J. Li, *Inorg. Chem.* 2010, **49**, 11276.
23 Y. Shen, D. D. Kuddes, C. A. Naquin, T. Hesterberg, C. Kusmierz, B. J. Holliday and J. D. Slinker, *Appl. Phys. Lett.* 2013, **102**, 203305.
24 K. Lin, L D. Bastatas, K. J. Suhr, M. D. Moore, B. J. Holliday and J. D. Slinker, *ACS Appl. Mater. Interfaces* 2016, **8**, 16776.
25 L. D. Bastatas, K. Lin, M. D. Moore, K. J. Suhr, M. H. Bowler, Y. Shen, B. J. Holliday and J. D. Slinker, *Langmuir* 2016, **32**, 9468.
26 E. Bandiello, M. Sessolo, and H. J. Bolink, *J. Mater. Chem. C*. 2016, **4**, 10781.
27 S. T. Parker, J. D. Slinker, M. S. Lowry, M. P. Cox, S. Bernhard, G.G. Malliaras, *Chem. Mater*. 2005, **17**, 3187.
28 R. D. Costa, A. Pertegas, E. Ortí and H. J. Bolink, *Chem. Mater*. 2010, **22**, 1288.
29 J. C. deMello, *Phys. Rev. B* 2002, **66**, 235210.
30 S. van Reenen, P. Matyba, A. Dzwilewski, R. A. Janssen, L. Edman and M. A. Kemerink, *J. Am. Chem. Soc.* 2010, **132**, 13776.
31 J. Gao and J. Dane *Appl. Phys. Lett.* 2003, **83**, 3027.
32 J. D. Slinker, J. A. DeFranco, M. J. Jaquith, W. R. Silveira, Y.-W. Zhong, J. M. Moran-Mirabal, H. G. Craighead, H. D. Abruna, J. A. Marohn and G. G. Malliaras, *Nature Mater*. 2007, **6**, 894-899.
33 L. D. Bastatas, M. D. Moore and J. D. Slinker, *ChemPlusChem* 2018, **83**, 266.
34 M. D. Weber, E. Fresta, M. Elie, M. E. Miehlich, J.-L. Renaud, K. Meyer, S. Gaillard and R. D. Costa, *Adv. Funct. Mater*. 2018, **28**, 1707423.
35 E. Fresta, G. Volpi, M. Milanesio, C. Garino, C. Barolo and R. D. Costa *Inorg. Chem.* 2018 **57**, 10469.
36 A. Sandström, P. Matyba, O. Inganäs and L. Edman, *J. Am. Chem. Soc.*, 2010, **132**, 6646.
37 K. T. Weber, K. Karikis, M. D. Weber, P. B. Coto, A. Charisiadis, D. Charitaki, G. Charalambidis, P. Angaridis, A. G. Coutsolelos and R. D. Costa, *Dalton Trans*. 2016, **45**, 13247.
38 E. Fresta and R. D. Costa, *J. Mater. Chem. C* 2017, **5**, 5643.
39 J. D. Slinker, J. Rivnay, J. S. Moskowitz, J. B. Parker, S. Bernhard, H. D. Abruna and G. G. Malliaras, *J. Mater. Chem.* 2007, **17**, 2976.
40 R. D. Costa, E. Ortí, H. J. Bolink, F. Monti, G. Accorsi, and N. Armaroli, *Angew. Chem. Int. Ed.* 2012, **51**, 8178.
41 T. Hu, L. He, L. Duan and Y. Qiu, *J. Mater. Chem.* 2012, **22**, 4206.
42 S. B. Meier, D. Tordera, A. Pertegas, C. Roldan-Carmona, E. Ortí and H. J. Bolink, *Mater. Today* 2014, **17**, 217.
43 C. Rothe, C.-J. Chiang, V. Jankus, K. Abdullah, X. Zeng, R. Jitchati, A. S. Batsanov, M. R. Bryce and A. P. Monkman, *Adv. Funct. Mater.*, 2009, **19**, 2038.
44 H.-C. Su, H.-F. Chen, F.-C. Fang, C.-C. Liu, C.-C. Wu, K.-T Wong, Y.-H. Liu and S.-M. Peng, *J. Am. Chem. Soc.* 2008, **130**, 3413.
45 J.-C. Leprêtre, A. Deronzier and O. Stéphan, *Synth. Met*. 2002, **131**, 175.
46 Wang, S.; Li, X.; Xun,, S.; Wan, X.; Wang, Z. Y. *Macromolecules* **2006**, *39*, 7502–7507.
47 Y.-M. Wang, F. Teng, Y.-B. Hou, Z. Xu, Y.-S. Wang and W.-F. Fu, *Appl. Phys. Lett.* 2005, **87**, 233512.
48 R. D. Costa, G. Fernández, L. Sánchez, N. Martín, E. Ortí and H. J. Bolink, *Chem. Eur. J.* 2010, **16**, 9855.
49 A. Aebischer, F. Gumy and J.-C. G. Bünzli, *Phys. Chem. Chem. Phys.* 2009, **11**, 1346.
50 CrysAlisPro, version 1.171.37.31; Rigaku Americas Corporation: The Woodlands, TX 77381, USA, 2016.
51 A. Altomare, M. C. Burla, M. Camalli, G. L. Cascarano, C. Giacovazzo, A. Guagliardi, A. G. G. Moliterni, G. Polidori and R. Spagna, *J. Appl. Crystallogr*. 1999, **32**, 115.
52 G. M. Sheldrick, *Acta Crystallogr*. 2008, **A64**, 112.
53 A. L. Spek, *J. Appl. Crystallogr*. 2003, **36**, 7.
54 L. J. Farrugia, *J. Appl. Cryst.* 2012, **45**, 849.
55 Mercury, version 3.8; The Cambridge Crystallographic Data Centre: Cambridge, UK, 2016.
56 POV-Ray, version 3.7.0; Persistence of Vision Raytracer Pty. Ltd.: Williamstown, Victoria 3016, Australia, 2013.

Table of Contents Image

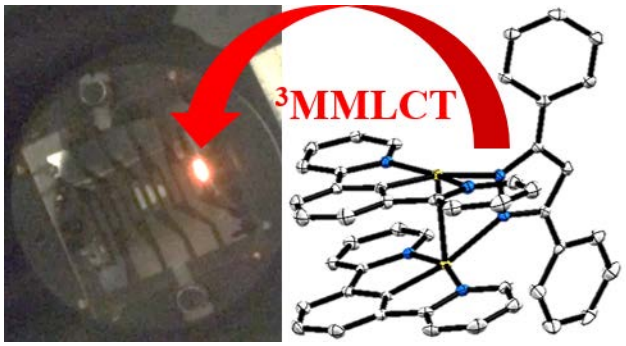

We report the synthesis, electrochemistry, photophysical properties and incorporation of a highly luminescent pyrazolate-bridged platinum (II) complex into light-emitting electrochemical devices. The absolute quantum yields of the complex in solution and the solid state at room temperate are 86% and 39%, respectively. Light-emitting electrochemical cells (LEECs) of this dimer complex were fabricated which displayed appreciable electroluminescence, among the brightest and most efficient LEECs from dinuclear compounds to date.